

pubs.acs.org/crystal Article

Effect of Fluorination on the Polymorphism and Photomechanical Properties of Cinnamalmalononitrile Crystals

Thomas J. Gately, Cameron Cook, Raghad Almuzarie, Imadul Islam, Zachary Gardner, Robbie J. Iuliucci, Rabih O. Al-Kaysi,* Gregory J. O. Beran,* and Christopher J. Bardeen*



Cite This: Cryst. Growth Des. 2022, 22, 7298-7307



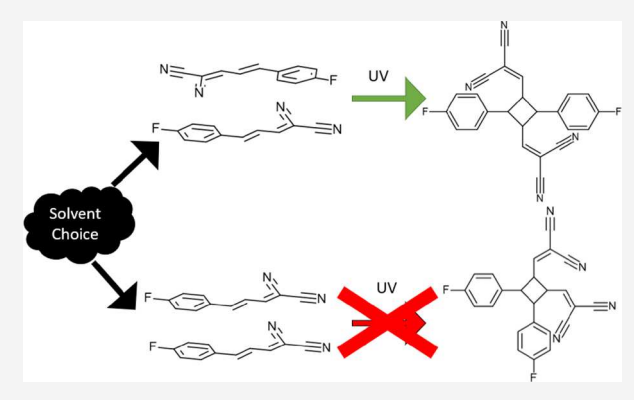
ACCESS I

III Metrics & More

Article Recommendations

Supporting Information

ABSTRACT: Cinnamalmalononitrile (CM) derivatives have been shown to exhibit a strong photomechanical response in the crystal form. In this paper, the effects of fluorine substitution on the molecular properties, crystal packing, and solid-state photochemical reactivity on this family of photochromes are explored. The addition of fluorines shifts the molecular $S_0 - S_1$ gap to a higher energy up to 0.4 eV. Fluorination also enables polymorphism in some of the derivatives that effectively controls whether or not they can undergo the [2 + 2] photodimerization. Depending on the substitution pattern, either the head-to-tail (HT, unreactive) or head-to-head (HH, reactive) crystal forms could be obtained. For some derivatives, both polymorphs could be grown depending on the solvent. Theoretical calculations on a subset of these molecules clarify how the fluorination of the CM framework modifies the polymorph landscape and shifts the energetics



of the different packing motifs. The CMs appear to support a rich polymorph landscape where HH and HT structures coexist within a few kJ/mol of each other, allowing the simple exchange of an aromatic H atom for an F atom to cause a complete loss of photomechanical activity due to changes in crystal packing. The experimental and computational results highlight how even minor modifications to the molecular structure can alter the resulting crystal structures and photomechanical behavior.

■ INTRODUCTION

In their pioneering studies of molecular crystal photochemistry, Schmidt and coworkers showed how the constraints of the crystalline environment can control the outcomes of chemical reactions. Their development of the topochemical principle has provided one of the cornerstones of solid-state chemistry. The intermolecular [2+2] photodimerization reaction played a central role in those studies. For example, Schmidt showed that different crystal polymorphs composed of the same molecule, trans-4-chlorocinnamic acid, could produce completely different reaction products, or no product at all, due to different crystal packing geometries. The [2+2] photodimerization continues to be widely studied as a prototypical crystal state chemical reaction, especially because of its relevance to solid-state kinetics.

From a practical standpoint, the topochemical principle can be exploited for organic synthesis. Crystalline [2+2] reactions have been used to prepare a variety of cyclobutane derivatives and polymers. In addition, the [2+2] photodimerization in molecular crystals can generate a mechanical response that takes many forms, like bending, photosalient behavior, and expansion. Although the limited reversibility of the [2+2] photodimerization probably prevents its wide adoption for practical actuators, it does have the ability to generate substantial

work. To demonstrate this, we recently grew crystalline nanowires of (E)-4-fluoro-cinnamalmalononitrile (4FCM) inside a porous anodic aluminum oxide template. This hybrid organic—inorganic composite could bend in response to 405 nm light that initiated the photodimerization inside the template. A few milligrams of embedded 4FCM could generate sufficient force to lift up to 400 g.

The CMs represent a novel class of photomechanical compounds that have demonstrated high reactivity and large force generation. Using this basic framework, it is important to establish whether it is possible to enhance the photomechanical response of this [2+2] photodimerization reaction by tuning the molecular structure. Fluorination is a well-established strategy for modifying crystal properties²⁹ and this strategy has been applied to other photomechanical systems based on the [2+2] dimerization.³⁰ In all these cases, fluorination resulted in changes in crystal packing and mechanical properties, but no

Received: August 16, 2022 Revised: October 19, 2022 Published: November 3, 2022





Table 1. Molecular Structures of the CM Derivatives Studied in this Paper along with their Abbreviations

N	N 		
N	N	N	
	F	F	
(E)-Cinnamalmalononitrile CM	(E)-2-Fluoro-cinnamalmalononitrile 2FCM	(E)-3-Fluoro-cinnamalmalononitrile 3FCM	
	z		
F	F	F	
(E)-4-Fluoro-cinnamalmalononitrile 4FCM	(E)-2,4-Difluoro- cinnamalmalononitrile 2,4FCM	(E)-3,5-Difluoro- cinnamalmalononitrile 3,5FCM	
F	N N N N N N N N N N N N N N N N N N N	N F F F	
(E)-2,6-Difluoro- cinnamalmalononitrile 2,6FCM	(E)-3,4,5-Trifluoro- cinnamalmalononitrile 3,4,5FCM	(E)-2,3,5,6-Tetrafluoro- cinnamalmalononitrile 2,3,5,6FCM	
F	z		
(E)-2,3,4,5,6-Pentafluoro- cinnamalmalononitrile 2,3,4,5,6FCM	(E)-4-Methoxy- cinnamalmalononitrile Methoxy-		

increased tendency toward polymorphism was reported. Thus the addition of fluorine atoms to the CM phenyl ring would seem to be a viable strategy to tune the crystal photomechanical response. Rather than the direct addition of fluorine to the phenyl ring of the CM, we can take advantage of the commercial availability of different fluorinated benzaldehydes and the Wittig coupling reaction to form the desired CM. This allows us to quickly explore a large space of fluorinated derivatives.

In this paper, we report the synthesis of multiple fluorinated CM derivatives and characterize their molecular properties, crystal packing, and solid-state photochemical reactivity. Our strategy is to vary the position and number of fluorine atoms on the benzene portion of the CM molecular frame. The CMs experience significant absorption blueshifts upon fluorination. We also find that fluorination enables polymorphism in some of the derivatives that effectively controls whether or not they can undergo the [2+2] photodimerization. Theoretical calculations on a subset of these molecules clarify how substituents on the CM framework can modify the polymorph landscape and shift the energetics of two different packing motifs, head-to-tail (HT) and head-to-head (HH). Since the HT motif is reactive and the

HH motif is unreactive, the polymorphism effectively determines whether the crystal exhibits photomechanical response. In some cases, the growth of different polymorphs can be controlled by solvent. Overall, the effect of fluorination on phenylbutadiene photomechanical crystals is qualitatively different from that on 9-anthracenecaboxylic acid (9AC) crystals, illustrating how chemical substitution can have dramatically different effects across different molecular photochrome families.

■ EXPERIMENTAL SECTION

Synthesis of the Fluorinated CM Derivatives. The detailed syntheses of the derivatives are provided in the Supporting Information section.

Crystal Growth. Crystals were grown either by simply allowing a concentrated solution to dry by evaporation, or by using ethanol hot water extraction. In the first case, growth by solvent evaporation was accomplished by putting 5 mg of the compound into a vial and dissolving the derivative in 2 mL of the desired solvent. Solvents used were chloroform, ethanol, methanol, toluene, ethyl acetate (EA), and dimethylformamide (DMF). The solvent was allowed to evaporate in the dark for a couple of days. The solution was placed in a refrigerator at

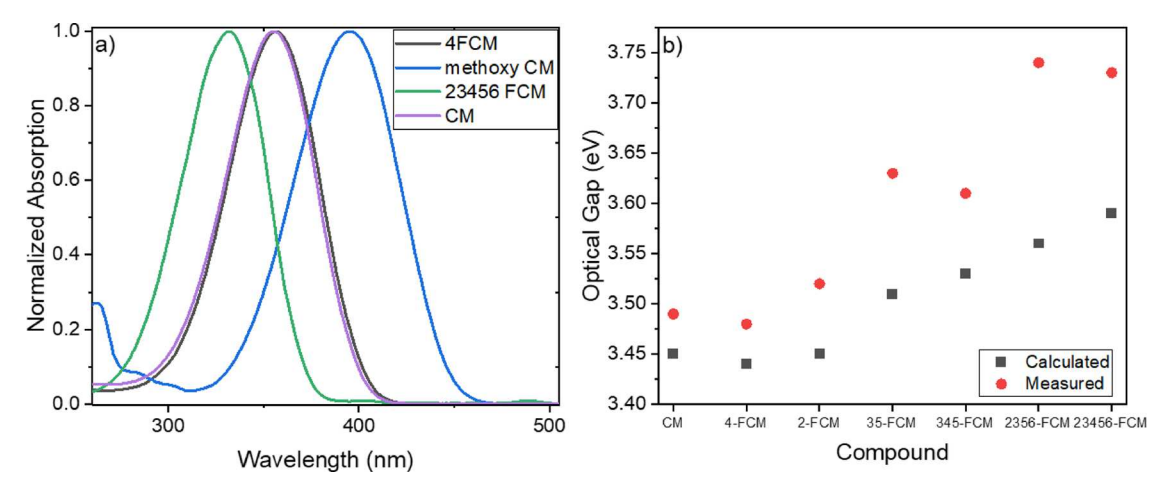


Figure 1. (a) Absorption spectra of unsubstituted CM, Methoxy-CM, 4FCM, and 2,3,4,5,6FCM. (b) Calculated (black squares) and experimental (red circles, measured at absorption peak) optical gaps for a subset of the CM derivatives studied in this paper.

 $4~^{\circ}\mathrm{C}$ or a furnace at $40~^{\circ}\mathrm{C}$ to slow or speed up the evaporation, depending on the solvent used. Hot water and ethanol extraction was performed by adding around 4 mg of the compound into a vial. Around 1 mL of ethanol was added, and the mixture was warmed to boiling. 1.5 mL of hot water was added to the ethanol solution, mixed slightly, then capped. The vial was allowed to cool down very slowly to room temperature while being protected from ambient light.

Crystal Structure Determination. The crystal structure of each derivative was obtained using a Bruker D8 Venture Duo diffractometer. Specific detectors, radiation, and refinement procedures varied depending on each molecule. The complete details of the X-ray diffraction analysis can be found in the Supporting Information. Note that the structure of **Methoxy-CM** has been reported previously³¹ and the structure determined in this paper is almost identical to that one.

Optical Microscopy. An Olympus IX70-inverted microscope with an Olympus IX-FLA fluorescence observation attachment was used to observe the crystals. Images and videos were obtained using an Amscope MU1000 camera.

UV–Vis Spectrospcopy. Samples were prepared by dissolving approximately 1 mg of each compound in 10 mL of chloroform. The solution was then placed into a quartz cuvette with a 1 cm pathlength and analyzed in a Cary 60 spectrometer from 200 to 800 nm.

Theoretical Calculations and Crystal Structure Prediction. Gas-phase calculations on dimer pairs and photodimers were performed using spin-component-scaled, dispersion-corrected second-order Møller–Plesset perturbation theory (SCS-MP2D), ³² using PSI4 v1.5³³ and the MP2D library. ³⁴ The results were extrapolated to the complete-basis-set (CBS) limit ³⁵ by combining HF/aug-cc-pVQZ with the extrapolation of the correlation energies computed in the aug-cc-pVTZ and aug-cc-pVQZ basis sets. ³⁶ The structures used in these calculations were either optimized in the gas-phase at the B3LYP/6-311+G* level of theory or taken from density functional theory (DFT)-optimized crystal structures (as described below).

Crystal structure prediction was carried out using a hierarchical procedure. CM and 4FCM were initially optimized in the gas phase at the B3LYP/6-311+G* level of theory. 84,000 random crystal packings from the 12 most common space groups for organic crystals (P1, P-1, $P2_1$, C2, Pc, Cc, $P2_1/c$, C2/c, $P2_12_12_1$, $Pca2_1$, $Pna2_1$, and Pbca) containing a single molecule in the asymmetric unit (Z'=1) were generated using PyXtal.³⁷ These structures were initially geometry optimized using the generalized Amber force field.³⁸ All crystal structures lying within 20 kJ/mol of the most stable structure on each landscape were then relaxed with the empirically corrected minimal basis set model, HF-3c,³⁹ as implemented in CRYSTAL17.⁴⁰ Next, the crystal structures lying within 10 kJ/mol of the minimum on the HF-3c landscape were optimized with periodic planewave DFT using the B86bPBE density functional^{37,41} and the exchange hole dipole moment (XDM) dispersion correction, 42 using Quantum Espresso v6.4. 43 The DFT calculations employed projector augmented wave potentials, a 50

Ry planewave cutoff, and a k-point spacing of 0.06 Å^{-1} . Given the similar structures of CM and 4FCM, we further enriched the two landscapes via "cross-pollination" to increase the completeness of the search: all structures from the 4FCM landscape structures had their fluorine replaced with hydrogen and were relaxed with DFT to place them on the CM landscape, while all CM structures were converted to 4FCM and similarly relaxed.

Because the CM and 4FCM molecules are not strictly planar and generalized gradient approximation density functionals like B86bPBE-XDM are known to exhibit biases toward certain conformations in systems with extended π -conjugation, final single point energies of the crystal structures were computed by employing an intramolecular energy correction which has previously been demonstrated to be important in a number of other polymorphic crystals. This correction adjusts the B86bPBE-XDM lattice energy based on the intramolecular energy difference computed with SCS-MP2D and B86bPBE-XDM (computed in the gas-phase using the molecular geometry directly extracted from each crystal):

$$E_{\text{crystal}}/Z = E_{\text{crystal}}(\text{DFT})/Z - E_{\text{molec}}(\text{DFT}) + E_{\text{molec}}(\text{SCS-MP2D})$$

See ref 50 for details. This correction shifted the relative lattice energies in CM and 4FCM by $1{-}2~\rm kJ/mol$, on average. After the removal of duplicate structures, the final CM and 4FCM crystal energy landscapes included 88 and 104 candidate crystal structures within the 10 kJ/mol thermodynamic energy window typically associated with organic crystal polymorphism. 51,52

Simulated optical gaps for CM and fluorinated derivatives were performed using time-dependent DFT (TDDFT). The derivatives were optimized in the gas phase at the BLYP-D3(BJ)/def2-TZVP level of theory using PSI4 v1.5. 35 TDDFT calculations were carried out with Ω B97X-D/def2-TZVP in a chloroform polarizable continuum model as implemented in Gaussian16 Rev. C.01. 53

RESULTS

Experimental Characterization of FCM Derivatives.

The syntheses of the molecules shown in Table 1 were carried out following a two-step process. First, the Wittig reaction was used to link a commercially available fluoro-benzaldehyde analog with ((1,3-dioxolan-2-yl)methyl)triphenylphosphonium bromide. Acid hydrolysis and purification by column chromatography, afforded the trans-fluorinated cinnamaldehyde analog. Second, the trans-fluorinated cinnamaldehyde derivative was condensed with excess malononitrile via the Knoevenagel condensation using ethanol/water as the solvent to afford the target compound in moderately high yields. This modular

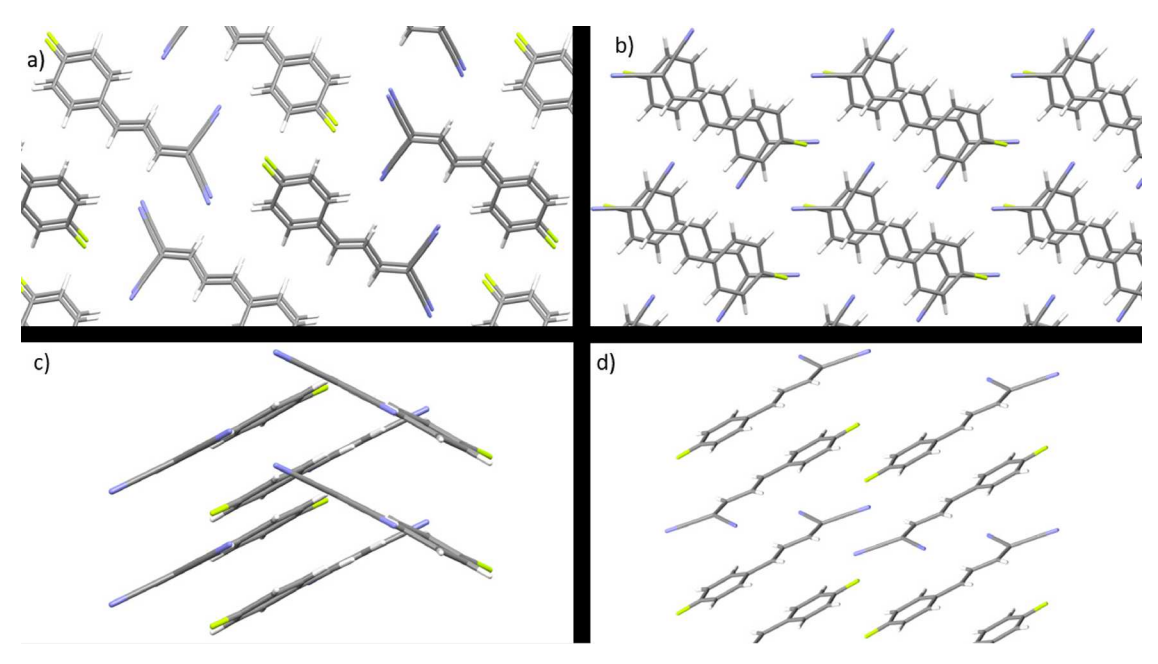


Figure 2. (a) Nonreactive **4FCM crystal** polymorph packs in a HH conformation. (b) Photoreactive crystal polymorph of **4FCM** packs in a HT conformation. Both (a) and (b) are views down the crystal *b*-axis. (c) Side view along the *c*-axis of the nonreactive **4FCM** HH packing. (d) Side view along the *a*-axis of the reactive **4FCM** HT packing.

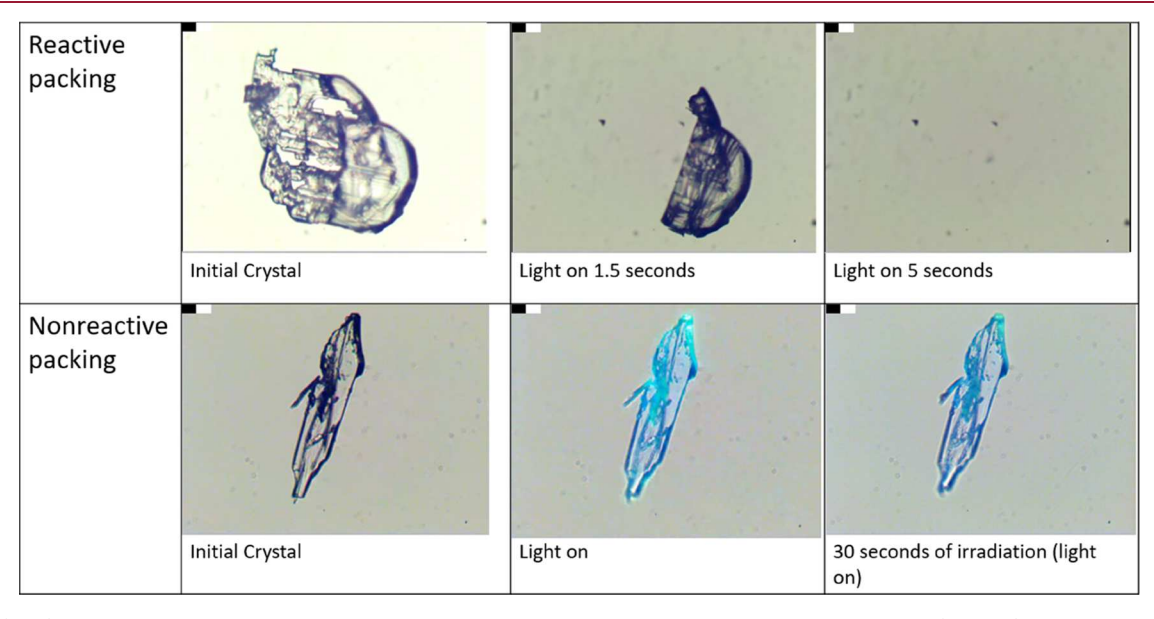


Figure 3. (Top) Photosalient 4FCM HT polymorph crystal quickly breaks apart when exposed to 405 nm light. (Bottom) Nonphotosalient 4FCM HH polymorph crystal yields a constant blue fluorescence and no mechanical response under the same illumination conditions. Scale bar is 50 μm.

synthetic strategy enabled the generation of a large family of substituted CM compounds.

The solution-phase absorption spectra of molecules in Table 1 provide the first indication that fluorine or methoxide substitution modifies their electronic structures. The absorption spectra of this class of molecules were strongly redshifted due to the cyano groups that terminate the butadiene. Previous studies have shown that the presence of these electron-withdrawing groups imparts some charge-transfer (CT) character to the excited state and lowers its energy. Adding an electron donating group like a methoxy to the phenyl ring enhances the CT nature of the excited state and the absorption spectrum shifts to a lower energy. When fluorines are added to the phenyl ring, it gains more electron withdrawing power that would be expected

to partially cancel out the electron withdrawing character of the CN groups. The net effect would be to lessen the CT character of the transition and shift the absorption to higher energies and shorter wavelengths. Indeed, this is what is observed in Figure 1a, where the 5 F atoms on 2,3,4,5,6FCM lead to the largest blue-shift of the absorption peak. The trend in observed $S_0 - S_1$ shifts is reasonably well-reproduced by TDDFT calculations, as shown in Figure 1b.

In addition to shifting the absorption spectra, fluorine substitution also modified the crystal packing. Two broad classes of packing motifs were identified and classified as HH and HT. Two molecules (4FCM, 2,3,4,5,6FCM) exhibited both HH and HT polymorphs, and 4FCM serves as a good representative example of both forms, as outlined in Figure 2.

The packing motifs for the other derivatives were similar and can be found in the Supporting Information. Both HH and HT forms consist of neighboring one-dimensional stacks of 4FCM molecules (Figure 2a,b). In the HH form, the phenyls are all aligned on the same side of the stack. In 4FCM, the HH stacks alternate orientations, so that each one makes a nonzero angle with respect to its neighbors (Figure 2c). This angling of the stacks depends on the compound, and in Methoxy-CM, the HH stacks are parallel. Although the double bonds lie within the 4.2 Å reaction range needed to support the [2+2] dimerization, the HH crystal is not reactive. The HT configuration, on the other hand, has the phenyl groups on alternate sides within the stack. Furthermore, the stacks are all aligned, so that the phenyl planes are all parallel (Figure 2d). This HT packing is similar to that of other phenylbutadiene derivatives that also exhibit [2 + 2]photodimerization in the crystal form.⁵⁷ This motif was reported in our earlier paper on 4FCM, but as we examined other derivatives and crystallization solvents, we found that the fluorinated derivatives can support both HH and HT crystal forms. 4FCM exhibited the HH polymorph when crystals were grown from nonhydrogen-bonding solvents (toluene, chloroform, EA, and acetone). When crystals were grown from hydrogen bonding solvents like methanol, ethanol, and DMF, the HT form was obtained. Crystallographic parameters for all compounds and polymorphs can be found in Table S1 in the Supporting Information.

The polymorph form, HH versus HT, controlled crystal reactivity. In all cases except one, the HT polymorph could undergo the [2+2] photodimerization reaction as judged from the disappearance of the fluorescence and NMR evidence for the photodimer (Supporting Information). All the reactive crystals showed a photomechanical response, usually taking the form of photosalient breaking and jumping. The sole exception to this rule was 2FCM, which grew in two HT polymorphs, one of which was unreactive due to a large intermolecular distance between the double bonds. In Figure 3, we contrast the behavior of the 4FCM HH and HT polymorphs. The crystal growth habits are quite different, as well as their response to 405 nm light. The HT polymorph is nonfluorescent and absorbs light until it suddenly cracks, and its fragments scatter outside the field of view. The HH polymorph, on the other hand, is fluorescent and remains stable for the duration of the light exposure. Videos showing the different responses can be found in the Supporting Information. Table 2 summarizes the results for all the CM derivatives and their reactivity, along with the solvents used for crystal growth. Note that we did not determine the crystal structure for all growth solvents, but the similar growth habits and reactivity within a class of solvents made it safe to assume that they generate the same crystal polymorph.

Examining Table 2, it is clear that the choice of solvent had a strong influence on whether a reactive polymorph was observed experimentally. For 2FCM and 4FCM, hydrogen-bonding solvents led to the photomechanical HT form, while other organic solvents led to either an unreactive HT form (2FCM) or the HH form (4FCM). Interestingly, this trend was reversed for 2,3,4,5,6FCM, where the HH form was favored in hydrogen-bonding solvents. Solvent control of polymorphism has been observed in other molecular systems and has been attributed to several different factors. Solvent control of polymorphism occurs when the molecule adopts different conformations in different solvents, with these different conformations leading to different packing geometries. However, examination of the crystal structures revealed that

Table 2. Solvent Growth Conditions Used to Obtain Polymorphs of the Various CM Derivatives^a

		1	1 . 1 . 1
1	1.	solvent for XRD	photomechanical
compound	packing	structure	response observed
CM	HT	Me	All
2FCM	HT (close)	Me	Me, Et, Et/ H_2O , DMF
	HT (far)	Cl	
3FCM	HH	Me	None
4FCM	HT	Me, Et	Me, Et, Et/ H_2O , DMF
	HH	Cl, T	
2,6FCM	HH	Cl	None
3,5FCM	HH	Et	None
2,4FCM	HT	Me	All
3,4,5FCM	HH	Me	None
2,3,5,6FCM	HH	Me	None
Methoxy-CM	HH	Me	None
2,3,4,5,6FCM	HT	Cl	Cl, T, EA, A
	HH	Me, Et	

^aMe is Methanol, Et is Ethanol, DMF is Dimethylformamide, T is Toluene, Cl is Chloroform, EA is Ethyl Acetate, A is Acetone, and Et/ H_2O is Ethanol and hot water extraction.

the 2FCM, 4FCM, and 2,3,4,5,6FCM molecules had similar conformations in all polymorphs. There was only a slight $(\pm 10^\circ)$ variation in twisting angles across the length of the molecule for all the derivatives. This slight twisting was not correlated with the solvent or crystal type, so we suspect that it reflects local stresses in the crystal packing arrangements, rather than a stable conformational change enabled by the solvent.

Crystal growth is a kinetic process and rapid nucleation can favor less stable polymorphs if they can assemble more quickly. Rapid solvent evaporation, low viscosity, and low solubility are all thought to favor rapid nucleation. In fact, a previous paper that observed solvent-dependent polymorphism in fluorinated aromatic compounds speculated that rapid solvent evaporation could favor a specific polymorph. However, attempts to correlate 4FCM polymorph formation with solvent vapor pressure and 4FCM solubility were unsuccessful, as shown in Figure 4a,b. HT formation does seem to correlate with solvent viscosity, as shown in Figure 4c. This correlation was not perfect, however, the more viscous toluene gave rise to the HH polymorph while ethanol gave rise to the HT form. Nevertheless, these data suggest that the properties of the solvent play a role in determining polymorph formation.

Computational Analysis of Crystal Polymorphism. The experimental observations described above raise several questions about the CM family of molecules that can be addressed using theoretical tools. The first question is why the HH polymorphs are unreactive. For the [2 + 2] dimerization to occur, the reacting π -bonds must have a center-to-center distance of less than 4.1 Å, the nominal cut-off for the [2 + 2]photodimerization. We found that in 4FCM and other derivatives, the HH polymorphs fulfilled this distance criterion but exhibited no reactivity. Since the cinnamates can be reactive in either arrangement, 6,7 the lack of reactivity in the HH polymorphs was surprising. For further insight, we investigated the gas-phase photodimerization of 4FCM in the HH and HT configurations using SCS-MP2D. While the HT monomer pair is about 5 kJ/mol more stable than the HH pair in the gas-phase, the photodimerization reaction energies are similar for both, at +14.9 and +16.3 kJ/mol for HT and HH, respectively (Figure 5a). In other words, the observed reactivity differences do not

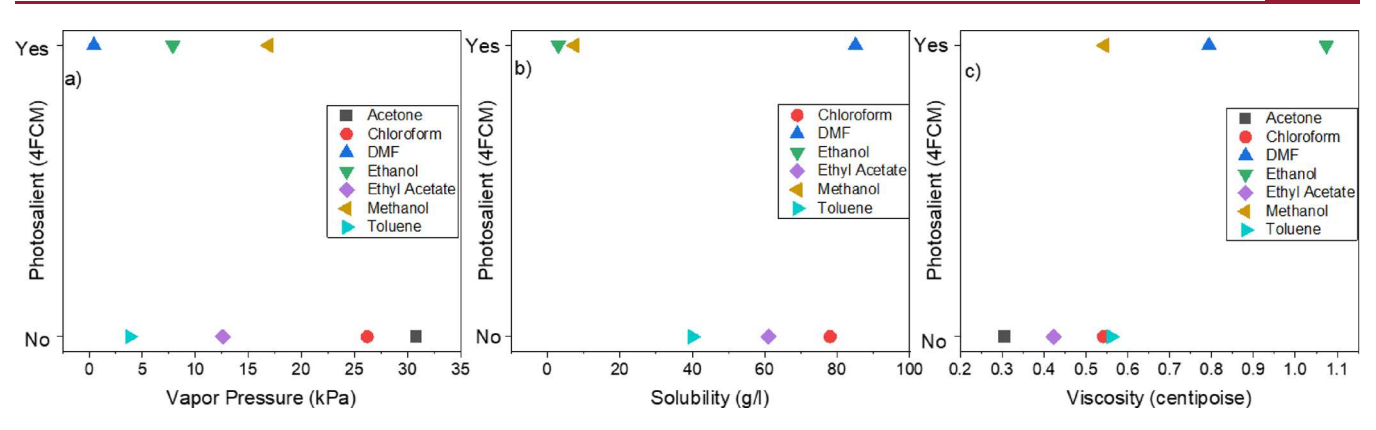


Figure 4. (a) Plot of the appearance of the photosalient (HT) crystal polymorph of **4FCM** as a function of the vapor pressure of the growth solvent. (b) Plot of the appearance of the photosalient (HT) crystal polymorph of **4FCM** as a function of the solubility of **4FCM** in the growth solvent. (c) Plot of the appearance of the photosalient (HT) crystal polymorph of **4FCM** as a function of the viscosity of the growth solvent.

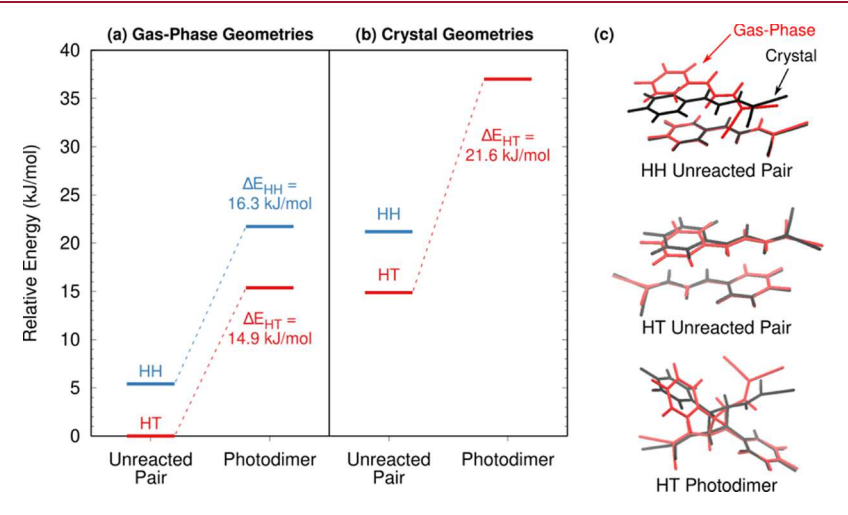


Figure 5. Relative energies of the HH and HT monomer pairs and the corresponding photodimers as computed using (a) gas-phase-optimized monomer pair geometries and (b) monomer pair geometries extracted from the DFT-relaxed experimental crystal structures. Energies are computed with SCS-MP2D/CBS. (c) Structure overlays comparing the gas-phase (red) and crystal (black) geometries. Changes in the molecular geometries due to the crystal packing impact the pair/photodimer energies significantly.

appear to stem from the thermodynamics of the isolated HH and HT dimer pair. The origin of the reactivity differences between the HH and HT polymorphs must be found in crystal packing effects, rather than at the molecular level.

In support of this hypothesis, we observe that the HH and HT unreacted pairs extracted from the DFT-optimized experimental 4FCM crystal structures lie 15–16 kJ/mol higher than the gasphase-optimized dimers (Figure 5b), while the HT photodimer from the solvent-grown photodimer crystal²⁸ lies more than 20 kJ/mol above its gas-phase-optimized analog. These substantial energy changes arise from clear differences in some of the dimer geometries (Figure 5c). For example, the gas-phase-optimized HH dimer stacks the two molecules with a 32° twist, in contrast to the parallel alignment found in the crystal. Similarly, the HT photodimer conformation extracted from the recrystallized material differs considerably from the gas-optimized one. Finally, whereas the monomer pairs in the reactive HT polymorph pack in planar sheets, the monomer pairs in the HH polymorph adopt a very different herringbone packing. In other words, crystal packing effects have a substantial impact on the molecular geometry and packing of 4FCM, and they would also be expected to play an important role in the energetics of photodimer formation. Determination of the full energetics of the photodimerization reaction in the crystal, including the

transition state, would be an interesting but challenging problem that is beyond the scope of the present work.

Given the influence of the crystal packing on whether the CM derivatives can undergo the [2 + 2] photodimerization and exhibit a photomechanical response, the next question is what controls this polymorphism? In an effort to understand how fluorination impacts the observed polymorphism, we turned to first-principles crystal structure prediction calculations. As limiting cases, we focused on CM, which always crystallizes in the same reactive HT polymorph, and 4FCM, which can grow in both reactive HT and nonreactive HH motifs, depending on the solvent. For simplicity, the crystal structure prediction search focused on structures containing only a single molecule in the asymmetric unit and residing in one of the 12 most common space groups. The final CM and 4FCM crystal energy landscapes contain 88 and 104 crystal structures within 10 kJ/ mol of the lowest-energy structure, respectively (Figure 6). After classifying the packing motifs based on whether they adopt HH or HT arrangements (albeit not necessarily within viable reaction distances), we find that CM prefers HH packing, with 61% HH structures on the landscape, 35% HT ones, and 4% alternative motifs. In contrast, 4FCM exhibits no clear preference for HH or HT packing, with the landscape being comprised of 47% HH, 51% HT, and 2% other structural motifs.

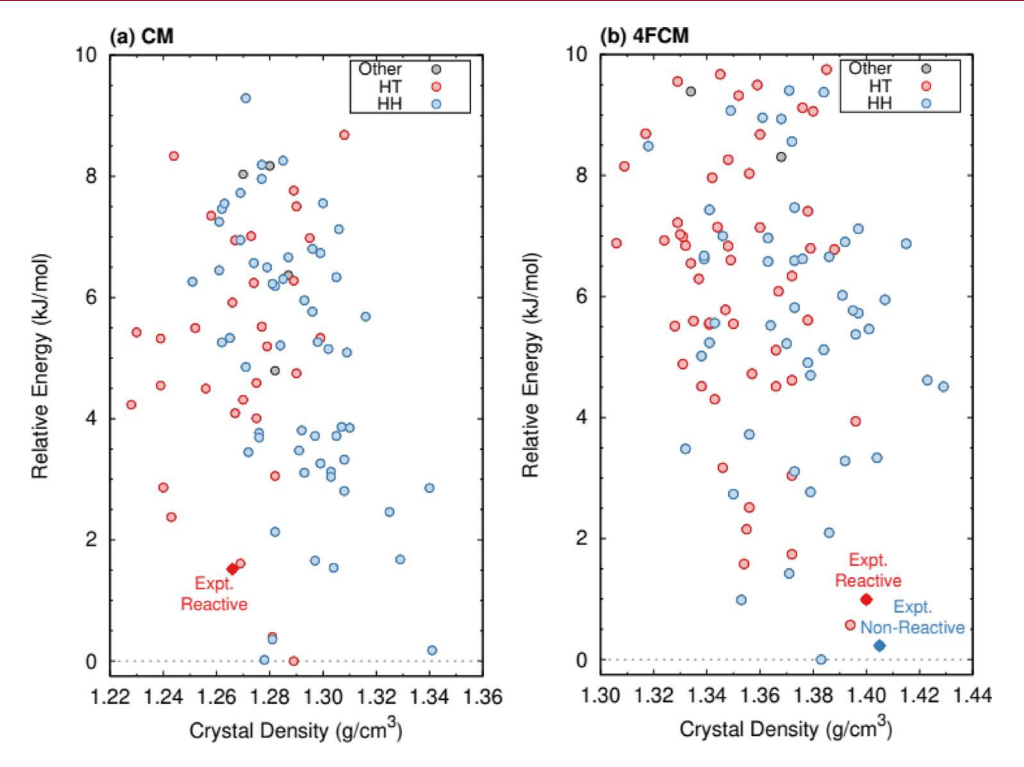


Figure 6. Predicted crystal energy landscapes for (a) **CM** and (b) **4FCM** at the B86bPBE-XDM DFT + intramolecular SCS-MP2D level of theory. Structures are classified as either HT (red) or HH (blue), where appropriate, and the experimentally known structures are labeled and indicated with solid diamond symbols. HH packing motifs are predicted to be much more common for **CM** than for **4FCM**.

Both crystal structure prediction searches produced the experimentally known crystal structures as low-energy structures. For CM (Figure 6a), the experimental structure occurs at Rank 6, lying 1.5 kJ/mol above the predicted global minimum energy structure. For 4FCM (Figure 6b), the experimentally observed HH and HT polymorphs occur at Ranks 2 (+0.2 kJ/mol) and 5 (+1.0 kJ/mol). For both species, the SCS-MP2D conformational energy correction improved the ranking of the experimentally known structures by 1–2 kJ/mol. Interestingly, the most stable predicted structure on the CM landscape shares the same packing as the 4FCM HT polymorph, while the Rank 4 CM structure matches the HH polymorph of 4FCM. The different observed crystal packing motifs in these two systems are all energetically competitive with each other.

Ideally, the lowest-energy structures on the crystal structure prediction landscape would match the experimentally observed polymorphs. This is not the case for CM and 4FCM, however, which may reflect non-zero temperature effects. On the one hand, a benchmark crystal structure prediction study of rigid, planar molecules which employed the same B86bPBE-XDM density functional used here found that the experimental structure was correctly predicted to be the global minimum lattice energy structure for 12 of 13 neutral species (often achieving sub-kJ/mol resolution between candidate structures).61 On the other hand, phonon contributions frequently impact the relative polymorph energies by up to 1-2 kJ/mol⁵² and could be sufficient to re-order the CM and 4FCM landscapes and stabilize the experimentally observed forms. Indeed, correct predictions for the 13th case in the aforementioned benchmark study were obtained once finitetemperature free energy effects were included. Whether all the minima in Figure 6 correspond to distinct polymorphs that can be isolated at room temperature is an open question. The main point is that crystal structure prediction demonstrates that both

CM and its 4-fluorinated analog can adopt a variety of energetically competitive crystal packing motifs. There is no obvious thermodynamic reason why 4FCM exhibits polymorphism while CM does not. In fact, our results suggest that CM does not have a strong thermodynamic preference for HT packing—HH motifs are actually much more common in the lower-energy region of the CM landscape.

DISCUSSION

In previous work, we found that the fluorination of 9AC had little effect on the molecular electronic properties, e.g., the optical gap, but did lead to photomechanical crystals with improved mechanical and photophysical properties. $^{62-64}$ All the derivatives studied in that work shared a similar crystal packing that allowed the [4+4] photodimerization reaction to proceed and no polymorphism was observed. For the 9ACs, the carboxylic acid group acts as a powerful director of crystal growth thanks to intermolecular hydrogen bonding. The **CM** frame lacks a strong crystal directing group, however, the expected effect of fluorination was less clear.

Indeed, we found that fluorine substitution on the CM family leads to a surprisingly rich landscape of polymorph crystal forms, only some of which are reactive. Attempts to rationalize polymorph formation on the basis of crystal energy calculations were not successful because the polymorphs were essentially indistinguishable. These results suggest that crystallization kinetics may be of central importance in determining which polymorphs occur experimentally. The viscosity dependence of 4FCM suggests that controlling the rate of crystal growth can favor different polymorphs. As mentioned above, however, the viscosity correlation is not perfect. A stronger correlation was found for hydrogen-bonding solvents, which always gave the same polymorph (HH or HT) for a given molecule. It is possible that solvent hydrogen bonding with the fluorinated phenyl ring

is strong enough to affect crystal growth kinetics. Some evidence for this is found by examining 3,5FCM, which only crystallized as a co-crystal with ethanol molecules localized around the phenyl ring (Supporting Information). This structure is consistent with the idea that the fluorinated phenyl ring provides an opportunity for solvent molecules to form transient hydrogen bonds. How such intermolecular bonds could steer polymorph growth is a subject for future investigation. Specific solvent-solute interactions have been shown to influence nucleation and crystal growth in other organic molecules, 65–67 although solvent-fluorine interactions have not been previously implicated in polymorph selection.

CONCLUSIONS

In this paper, we explored how fluorine substitution affects the electronic states and crystal packing in a family of CM derivatives. First, the addition of fluorines can shift the $S_0 - S_1$ energy gap by up to 0.4 eV. Second, depending on the substitution pattern, either the HH (unreactive) or HT (reactive) crystal forms could be obtained. For some derivatives, both polymorphs could be grown depending on the solvent. The polymorphism and solvent control were surprising to us at first, given our previous experience with the anthracene carboxylic family where the F atoms appeared to be innocent bystanders from the perspective of molecular energy gaps and crystal packing. In the case of the CMs, however, the simple exchange of an aromatic H atom for an F atom can cause a complete loss of photomechanical activity due to changes in crystal packing. Computational work confirms that the fluorinated CMs can give rise to a rich polymorph landscape where HH and HT structures can coexist within a few kJ/mol of each other. It is probable that both thermodynamic and kinetic factors play significant roles in determining which polymorphs are observed for this class of compounds. The experimental and computational results highlight the difficulty of trying to anticipate how even minor modifications to the molecular structure will alter the resulting crystal structures, especially in the absence of strong directing groups/synthons like COOH. Future efforts to create more powerful organic photomechanical crystals will rely on progress in molecular design combined with an improved understanding of crystal engineering and crystal growth.

ASSOCIATED CONTENT

Supporting Information

The Supporting Information is available free of charge at https://pubs.acs.org/doi/10.1021/acs.cgd.2c00930.

Detailed synthesis of the fluorinated **CM** derivatives; complete details of the X-ray diffraction analysis; packing motifs for the other derivatives; and crystallographic parameters for all compounds and polymorphs (PDF)

2FCM nonreactive black and white (MP4)

2FCM reactive 4 (MP4)

4FCM nonreactive dark (MP4)

4FCM reactive 9 (MP4)

2,3,4,5,6FCM 405 photosalient black and white (MP4)

2,3,4,5,6FCM nonreactive (MP4)

Accession Codes

CCDC 2182921—2182932 contain the supplementary crystallographic data for this paper. These data can be obtained free of charge via www.ccdc.cam.ac.uk/data_request/cif, or by emailing data_request@ccdc.cam.ac.uk, or by contacting The Cam-

bridge Crystallographic Data Centre, 12 Union Road, Cambridge CB2 1EZ, UK; fax: +44 1223 336033.

AUTHOR INFORMATION

Corresponding Authors

Rabih O. Al-Kaysi — College of Science and Health Professions-3124, King Saud bin Abdulaziz University for Health Sciences, and King Abdullah International Medical Research Center (Nanomedicine), Ministry of National Guard Health Affairs, Riyadh 11426, Kingdom of Saudi Arabia;

Email: rabihalkaysi@gmail.com

Gregory J. O. Beran — Department of Chemistry, University of California, Riverside, California 92521, United States;
orcid.org/0000-0002-2229-2580;

Email: gregory.beran@ucr.edu

Christopher J. Bardeen – Department of Chemistry, University of California, Riverside, California 92521, United States;

orcid.org/0000-0002-5755-9476; Email: christopher.bardeen@ucr.edu

Authors

Thomas J. Gately — Department of Chemistry, University of California, Riverside, California 92521, United States;
o orcid.org/0000-0001-6199-4764

Cameron Cook – Department of Chemistry, University of California, Riverside, California 92521, United States

Raghad Almuzarie — College of Science and Health Professions-3124, King Saud bin Abdulaziz University for Health Sciences, and King Abdullah International Medical Research Center (Nanomedicine), Ministry of National Guard Health Affairs, Riyadh 11426, Kingdom of Saudi Arabia

Imadul Islam — College of Science and Health Professions-3124,
 King Saud bin Abdulaziz University for Health Sciences, and
 King Abdullah International Medical Research Center
 (Nanomedicine), Ministry of National Guard Health Affairs,
 Riyadh 11426, Kingdom of Saudi Arabia

Zachary Gardner — Department of Chemistry, Washington and Jefferson College, Washington, Pennsylvania 15301, United States

Robbie J. Iuliucci — Department of Chemistry, Washington and Jefferson College, Washington, Pennsylvania 15301, United States; Occid.org/0000-0001-6714-1842

Complete contact information is available at: https://pubs.acs.org/10.1021/acs.cgd.2c00930

Notes

The authors declare no competing financial interest.

■ ACKNOWLEDGMENTS

C.J.B. acknowledges support from the Office of Naval Research (MURI on Photomechanical Material Systems; ONR N00014-18-1-2624). R.O.K. acknowledges the support of KSAU-HS/KAIMRC through grant NRC21R25003. G.J.O.B. acknowledges support from the National Science Foundation (CHE-1955554) and supercomputer time from XSEDE (TG-CHE110064). R.J.I. acknowledges support from a Research Opportunity Award supplement to CHE-1955554 and REU CHE-1950585.

REFERENCES

(1) Schmidt, G. M. J. Photodimerization in the Solid State. *Pure Appl. Chem.* 1971, 27, 647–678.

- (2) Cohen, M. D. The Photochemistry of Organic Solids. Angew. Chem., Int. Ed. 1975, 14, 386-393.
- (3) Ramamurthy, V.; Venkatesan, K. Photochemical Reactions of Organic Crystals. *Chem. Rev.* **1987**, 87, 433–481.
- (4) Boldyrev, V. V. Topochemistry and topochemical reactions. *React. Solids* **1990**, *8*, 231–246.
- (5) Biradha, K.; Santra, R. Crystal engineering of topochemical solid state reactions. *Chem. Soc. Rev.* **2013**, *42*, 950–967.
- (6) Cohen, M. D.; Schmidt, G. M. J.; Sonntag, F. I. Topochemistry Part II. The Photochemistry of trans-Cinnnamic Acids. *J. Chem. Soc.* 1964, 2000–2013.
- (7) Schmidt, G. M. J. Topochemistry Part III. The Crystal Chemistry of Some trans-Cinnamic Acids. *J. Chem. Soc.* **1964**, 2014–2021.
- (8) Friscic, T.; MacGillivray, L. R. Single-Crystal-to-Crystal [2+2] Photodimerization: from Discovery to Design. *Z. Kristallogr.* **2005**, 220, 351–363.
- (9) Davaasambuu, J.; Busse, G.; Techert, S. Aspects of the Photodimerization Mechanism of 2,4-Dichlorocinnamic Acid Studied by Kinetic Photocrystallography. *J. Phys. Chem. A* **2006**, *110*, 3261–3265.
- (10) Benedict, J. B.; Coppens, P. Kinetics of the Single-Crystal to Single-Crystal Two-Photon Photodimerization of α -trans-Cinnamic Acid to α -Truxillic Acid. J. Phys. Chem. A **2009**, 113, 3116–3120.
- (11) Atkinson, S. D. M.; Almond, M. J.; Hibble, S. J.; Hollins, P.; Jenkins, S. L.; Tobin, M. J.; Wiltshire, K. S. An in situ time-dependent study of the photodimerisation of chloro-derivatives of trans-cinnamic acid using infrared microspectroscopy with a synchrotron radiation source. *Phys. Chem. Chem. Phys.* **2004**, *6*, 4–6.
- (12) Khan, M.; Brunklaus, G.; Enkelmann, V.; Spiess, H. W. Transient states in the [2+2] photodimerization of cinnamic acid: correlation of solid-state NMR and X-ray analysis. *J. Am. Chem. Soc.* **2008**, *130*, 1741–1748.
- (13) Nieuwendaal, R. C.; Bertmer, M.; Hayes, S. E. An unexpected phase transition during the [2+2] photocycloaddition reaction of cinnamic acid to truxillic acid: changes in polymorphism monitored by solid state NMR. *J. Phys. Chem. B* **2008**, *112*, 12920–12926.
- (14) Bertmer, M.; Nieuwendaal, R. C.; Barnes, A. B.; Hayes, S. E. Solid-state photodimerization kinetics of a-trans-cinnamic acid to a-truxillic acid studied via solid-state NMR. *J. Phys. Chem. B* **2006**, *110*, 6270–6273.
- (15) Panda, T.; Naumov, P. Time-Dependent Photodimerization of α -trans-Cinnamic Acid Studied by Photocalorimetry and NMR Spectroscopy. *Cryst. Growth Des.* **2018**, *18*, 2744–2749.
- (16) MacGillivray, L. R.; Papaefstathiou, G. S.; Friscic, T.; Hamilton, T. D.; Bucar, D. K.; Chu, Q.; Varshney, D. B.; Georgiev, I. G. Supramolecular control of reactivity in the solid state: from templates to ladderanes to metal-organic frameworks. *Acc. Chem. Res.* **2008**, *41*, 280–291.
- (17) Hema, K.; Ravi, A.; Raju, C.; Pathan, J. R.; Rai, R.; Sureshan, K. M. Topochemical polymerizations for the solid-state synthesis of organic polymers. *Chem. Soc. Rev.* **2021**, *50*, 4062–4099.
- (18) Naumov, P.; Kowalik, J.; Solntsev, K. M.; Baldridge, A.; Moon, J.-S.; Kranz, C.; Tolbert, L. M. Topochemistry and photomechanical effects in crystals of green fluorescent protein-like chromophores: effects of hydrogen bonding and crystal packing. *J. Am. Chem. Soc.* **2010**, 132, 5845–5857.
- (19) Kim, T.; Zhu, L.; Mueller, L. J.; Bardeen, C. J. Dependence of the solid-state photomechanical response of 4-chlorocinnamic acid on crystal shape and size. *CrystEngComm* **2012**, *14*, 7792–7799.
- (20) Medishetty, R.; Husain, A.; Bai, Z.; Runceviski, T.; Dinnebier, R. E.; Naumov, P.; Vittal, J. J. Single crystals popping under UV light: a photosalient effect triggered by a [2+2] cycloaddition reaction. *Angew. Chem., Int. Ed.* **2014**, *53*, 5907–5911.
- (21) Kole, G. K.; Kojima, T.; Kawano, M.; Vittal, J. J. Reversible Single-Crystal-to-Single-Crystal Photochemical Formation and Thermal Cleavage of a Cyclobutane Ring. *Angew. Chem., Int. Ed.* **2014**, 53, 2143–2146.

- (22) Medishetty, R.; Sahoo, S. C.; Mulijanto, C. E.; Naumov, P.; Vittal, J. J. Photosalient Behavior of Photoreactive Crystals. *Chem. Mater.* **2015**, 27, 1821–1829.
- (23) Yadava, K.; Vittal, J. J. Photosalient Behavior of Photoreactive Zn(II) Complexes. *Cryst. Growth Des.* **2019**, *19*, 2542–2547.
- (24) Rath, B. B.; Vittal, J. J. Photoreactive Crystals Exhibiting [2 + 2] Photocycloaddition Reaction and Dynamic Effects. *Acc. Chem. Res.* **2022**, *55*, 1445–1455.
- (25) Wang, H.; Chen, P.; Wu, Z.; Zhao, J.; Sun, J.; Lu, R. Bending, Curling, Rolling, and Salient Behavior of Molecular Crystals Driven by [2+2] Cycloaddition of a Styrylbenzoxazole Derivative. *Angew. Chem., Int. Ed.* **2017**, *56*, 9463–9467.
- (26) Peng, J.; Ye, K.; Liu, C.; Sun, J.; Lu, R. The photomechanic effects of the molecular crystals based on 5-chloro-2-(naphthalenylvinyl)-benzoxazols fueled by topo-photochemical reactions. *J. Mater. Chem. C* **2019**, *7*, 5433–5441.
- (27) Shen, J. L. K. Y. Y.; Peng, J.; Sun, J.; Lu, R. Photoactuators based on the dynamic molecular crystals of naphthalene acrylic acids driven by stereospecific [2+2] cycloaddition reactions. *J. Mater. Chem. C* **2020**, *8*, 3165–3175.
- (28) Tong, F.; Xu, W.; Guo, T.; Lui, B. F.; Hayward, R. C.; Palffy-Muhoray, P.; Al-Kaysi, R. O.; Bardeen, C. J. Photomechanical molecular crystals and nanowire assemblies based on the [2+2] photodimerization of a phenylbutadiene derivative. *J. Mater. Chem. C* **2020**, *8*, 5036–5044.
- (29) Reichenbacher, K.; Suss, H. I.; Hulliger, J. Fluorine in crystal engineering—"the little atom that could". *Chem. Soc. Rev.* **2005**, *34*, 22–30.
- (30) Shu, Y.; Ye, K.; Yue, Y.; Sun, J.; Wang, H.; Zhong, J.; Yang, X.; Gao, H.; Lu, R. Fluorine as a robust balancer for tuning the reactivity of topo-photoreactions of chalcones and the photomechanical effects of molecular crystals. *CrystEngComm* **2021**, 5856–5868.
- (31) Antipin, M. Y.; Timofeeva, T. V.; Clark, R. D.; Nesterov, V. N.; Sanghadasa, M.; Barr, T. A.; Penn, B.; Romero, L.; Romero, M. Molecular Crystal Structures and Nonlinear Optical Properties in the Series of Dicyanovinylbenzene and Its Derivatives. *J. Phys. Chem. A* **1998**, *102*, 7222–7232.
- (32) Greenwell, C.; Řezáč, J.; Beran, G. J. O. Spin-component-scaled and dispersion-corrected second-order Møller—Plesset perturbation theory: a path toward chemical accuracy. *Phys. Chem. Chem. Phys.* **2022**, 24, 3695—3712.
- (33) Smith, D. G. A.; Burns, L. A.; Simmonett, A. C.; Parrish, R. M.; Schieber, M. C.; Galvelis, R.; Kraus, P.; Kruse, H.; Remigio, R. D.; Alenaizan, A.; James, A. M.; Lehtola, S.; Misiewicz, J. P.; Scheurer, M.; Shaw, R. A.; Schriber, J. B.; Xie, Y.; Glick, Z. L.; Sirianni, D. A.; O'Brien, J. S.; Waldrop, J. M.; Kumar, A.; Hohenstein, E. G.; Pritchard, B. P.; Brooks, B. R.; Sokolov, A. Y.; Patkowski, K.; Bozkaya, U.; King, R. A.; Evangelista, F. A.; Turney, J. M.; Crawford, T. D.; Sherrill, C. D. PSI4 1.4: Open-source software for high-throughput quantum chemistry. *J. Chem. Phys* 2020, 152, 184108.
- (34) github, this is a placeholder, 2022.
- (35) Helgaker, T.; Klopper, W.; Koch, H.; Noga, J. Basis-set convergence of correlated calculations on water. *J. Chem. Phys.* **1997**, 106, 9639–9646.
- (36) Dunning, T. H. Gaussian basis sets for use in correlated molecular calculations I. The atoms boron through neon and hydrogen. *J. Chem. Phys.* **1989**, 90, 1007–1023.
- (37) Fredericks, S.; Parrish, K.; Sayre, D.; Zhu, Q. PyXtal: A Python library for crystal structure generation and symmetry analysis. *Comput. Phys. Commun.* **2021**, *261*, No. 107810.
- (38) Wang, J.; Wolf, R. M.; Caldwell, J. W.; Kollman, P. A.; Case, D. A. Development and testing of a general amber force field. *J. Comput. Chem.* **2004**, 25, 1157–1174.
- (39) Sure, R.; Grimme, S. Corrected small basis set Hartree-Fock method for large systems. *J. Comput. Chem.* **2013**, 34, 1672–1685.
- (40) Dovesi, R.; Erba, A.; Orlando, R.; Zicovich-Wilson, C. M.; Civalleri, B.; Maschio, L.; Rérat, M.; Casassa, S.; Baima, J.; Salustro, S.; Kirtman, B. Quantum-mechanical condensed matter simulations with CRYSTAL. WIREs Comput. Mol. Sci. 2018, 8, No. e1360.

- (41) Becke, A. D. On the large-gradient behavior of the density functional exchange energy. *J. Chem. Phys.* **1986**, *85*, 7184–7187.
- (42) Otero-de-la-Roza, A.; Johnson, E. R. Van der Waals interactions in solids using the exchange-hole dipole moment model. *J. Chem. Phys.* **2012**, *136*, 174109.
- (43) Giannozzi, P.; Andreussi, O.; Brumme, T.; Bunau, O.; Nardelli, M. B.; Calandra, M.; Car, R.; Cavazzoni, C.; Ceresoli, D.; Cococcioni, M.; Colonna, N.; Carnimeo, I.; Corso, A. D.; Gironcoli, S. d.; Delugas, P.; DiStasio, R. A., Jr; Ferretti, A.; Floris, A.; Fratesi, G.; Fugallo, G.; Gebauer, R.; Gerstmann, U.; Giustino, F.; Gorni, T.; Jia, J.; Kawamura, M.; Ko, H.-Y.; Kokalj, A.; Küçükbenli, E.; Lazzeri, M.; Marsili, M.; Marzari, N.; Mauri, F.; Nguyen, N. L.; Nguyen, H.-V.; Otero-de-la-Roza, A.; Paulatto, L.; Poncé, S.; Rocca, D.; Sabatini, R.; Santra, B.; Schlipf, M.; Seitsonen, A. P.; Smogunov, A.; Timrov, I.; Thonhauser, T.; Umari, P.; Vast, N.; Wu, X.; Baroni, S. Advanced capabilities for materials modelling with Quantum ESPRESSO. J. Phys.: Condens. Matter 2017, 29, 465901.
- (44) Greenwell, C.; Beran, G. J. O. Inaccurate Conformational Energies Still Hinder Crystal Structure Prediction in Flexible Organic Molecules. *Cryst. Growth Des.* **2020**, *20*, 4875–4881.
- (45) Greenwell, C.; McKinley, J. L.; Zhang, P.; Zeng, Q.; Sun, G.; Li, B.; Wen, S.; Beran, G. J. O. Overcoming the difficulties of predicting conformational polymorph energetics in molecular crystals via correlated wavefunction methods. *Chem. Sci.* **2020**, *11*, 2200–2214.
- (46) Greenwell, C.; Beran, G. J. O. Rubrene untwisted: common density functional theory calculations overestimate its deviant tendencies. *J. Mater. Chem. C* **2021**, *9*, 2848–2857.
- (47) Beran, G. J. O. Solid state photodimerization of 9-tert-butyl anthracene ester produces an exceptionally metastable polymorph according to firstprinciples calculations. *Cryst. Eng. Commun.* **2019**, 21, 758–764.
- (48) Beran, G. J. O.; Sugden, I. J.; Greenwell, C.; Bowskill, D. H.; Pantelides, C. C.; Adjiman, C. S. How many more polymorphs of ROY remain undiscovered. *Chem. Sci.* **2022**, *13*, 1288–1297.
- (49) Beran, G. J. O.; Wright, S. E.; Greenwell, C.; Cruz-Cabeza, A. J. The interplay of intra- and intermolecular errors in modeling conformational polymorphs. *J. Chem. Phys.* **2022**, *156*, 104112.
- (50) Giulini, M.; Menichetti, R.; Shell, M. S.; Potestio, R. An Information-Theory-Based Approach for Optimal Model Reduction of Biomolecules. *J. Chem. Theory Comput.* **2020**, *16*, 6795–6813.
- (51) Cruz-Cabeza, A. J.; Reutzel-Edens, S. M.; Bernstein, J. Facts and fictions about polymorphism. *Chem. Soc. Rev.* **2015**, *44*, 8619–8635.
- (52) Nyman, J.; Day, G. M. Static and lattice vibrational energy differences between polymorphs. *CrystEngComm* **2015**, *17*, 5154–5165.
- (53) Frisch, M. J.; Trucks, G. W.; Schlegel, H. B.; Scuseria, G. E.; Robb, M. A.; Cheeseman, J. R.; Scalmani, G.; Barone, V.; Petersson, G. A.; Nakatsuji, H.; Li, X.; Caricato, M.; Marenich, A. V.; Bloino, J.; Janesko, B. G.; Gomperts, R.; Mennucci, B.; Hratchian, H. P.; Ortiz, J. V.; Izmaylov, A. F.; Sonnenberg, J. L.; Williams-Young, D.; Ding, F.; Lipparini, F.; Egidi, F.; Goings, J.; Peng, B.; Petrone, A.; Henderson, T.; Ranasinghe, D.; Zakrzewski, V. G.; Gao, J.; Rega, N.; Zheng, G.; Liang, W.; Hada, M.; Ehara, M.; Toyota, K.; Fukuda, R.; Hasegawa, J.; Ishida, M.; Nakajima, T.; Honda, Y.; Kitao, O.; Nakai, H.; Vreven, T.; Throssell, K.; Montgomery, J. A.; Peralta, J. E., Jr.; Ogliaro, F.; Bearpark, M. J.; Heyd, J. J.; Brothers, E. N.; Kudin, K. N.; Staroverov, V. N.; Keith, T. A.; Kobayashi, R.; Normand, J.; Raghavachari, K.; Rendell, A. P.; Burant, J. C.; Iyengar, S. S.; Tomasi, J.; Cossi, M.; Millam, J. M.; Klene, M.; Adamo, C.; Cammi, R.; Ochterski, J. W.; Martin, R. L.; Morokuma, K.; Farkas, O.; Foresman, J. B.; Fox, D. J. Gaussian 16, Revision C.01; Gaussian, Inc.: Wallingford CT, 2016.
- (54) Aihara, J.-I.; Araya, K.; Chiba, K.; Matsunaga, Y. Characterization of intramolecular charge-transfer transitions: 2,2-dicyanovinylaromatics. *Adv. Molec. Interact. Relax. Proc.* **1980**, *18*, 199–210.
- (55) Reddy, M. J. R.; Rao, G. V.; Bushan, K. M.; Reddy, M. J. R.; Gopal, V. R.; Rao, V. J. Wavelength Dependent Regioselective E(trans)→Z(cis) Photoisomerization in Anthryldienes. *Chem. Lett.* **2001**, *30*, 186–187.

- (56) Srinivas, U.; Kumar, P. A.; Srinivas, K.; Bhanuprakash, K.; Rao, V. J. Conformational analysis of 2-anthryl-ethylene derivatives: Photochemical and computational investigation. *J. Struct. Chem.* **2012**, *53*, 851–865.
- (57) Row, T. N. C.; Swamy, H. R.; Acharyaa, K. R.; Ramamurthy, V.; Venkatesan, K.; Rao, C. N. R. Reversible Photodimerization of Phenylbutadienes in the Solid State. *Tetrahedron Lett.* **1983**, 3263–3266.
- (58) Kitamura, M. Strategy for control of crystallization of polymorphs. CrystEngComm 2009, 11, 949–964.
- (59) Nangia, A. Conformational Polymorphism in Organic Crystals. *Acc. Chem. Res.* **2008**, *41*, 595–604.
- (60) Kusukawa, T.; Kannen, F.; Kojima, Y.; Yoza, K. Crystal Polymorphism-dependent Fluorescence of Fluoroarene-substituted Anthracene Derivatives. *Chem. Lett.* **2021**, *50*, 31–34.
- (61) Whittleton, S. R.; Otero-de-la-Roza, A.; Johnson, E. R. Exchange-Hole Dipole Dispersion Model for Accurate Energy Ranking in Molecular Crystal Structure Prediction. *J. Chem. Theory Comput.* **2017**, 13, 441–450.
- (62) Zhu, L.; Al-Kaysi, R. O.; Dillon, R. J.; Tham, F. S.; Bardeen, C. J. Crystal structures and photophysical properties of 9-anthracene carboxylic acid derivatives for photomechanical applications. *Cryst. Growth Des.* **2011**, *11*, 4975–4983.
- (63) Zhu, L.; Tong, F.; Salinas, C.; Al-Muhanna, M. K.; Tham, F. S.; Kisailus, D.; Al-Kaysi, R. O.; Bardeen, C. J. Improved Solid-State Photomechanical Materials by Fluorine Substitution of 9-Anthracene Carboxylic Acid. *Chem. Mater.* **2014**, *26*, 6007–6015.
- (64) Gately, T. J.; Sontising, W.; Easley, C. J.; Islam, I.; Al-Kaysi, R. O.; Beran, G. J. O.; Bardeen, C. J. Effect of halogen substitution on energies and dynamics of reversible photomechanical crystals based on 9-anthracenecarboxylic acid. *CrystEngComm* **2021**, *23*, 5931–5943.
- (65) Zeglinski, J.; Kuhs, M.; Khamar, D.; Hegarty, A. C.; Devi, R. K.; Rasmuson, A. C. Crystal Nucleation of Tolbutamide in Solution: Relationship to Solvent, Solute Conformation, and Solution Structure. *Chem. Eur. J.* **2018**, *24*, 4916–4926.
- (66) Ouyang, J.; Chen, J.; Rosbottom, I.; Chen, W.; Guo, M.; Heng, J. Y. Supersaturation and solvent dependent nucleation of carbamazepine polymorphs during rapid cooling crystallization. *CrystEngComm* **2021**, 23, 813–823.
- (67) Kakkar, S.; Devi, K. R.; Rasmuson, Å. C. Molecular Clustering of Fenoxycarb and Salicylic Acid in Organic Solvents and Relation to Crystal Nucleation. *Cryst. Growth Des.* **2022**, *22*, 2824–2836.